Journal of
Mechanics of
Materials and Structures

INCREMENTAL MODELING OF T-STUB CONNECTIONS

Minas E. Lemonis and Charis J. Gantes

Volume 1, Nº 7 September 2006

mathematical sciences publishers

JOURNAL OF MECHANICS OF MATERIALS AND STRUCTURES
Vol. 1, No. 7, 2006
dx.doi.org/10.2140/jomms.2006.1.1135

msp

INCREMENTAL MODELING OF T-STUB CONNECTIONS

MINAS E. LEMONIS AND CHARIS J. GANTES

An incremental model for predicting the mechanical characteristics of T-stub steel connections is presented in this paper. The response is calculated analytically on the basis of a simple beam representation for the flange and a deformational spring for the bolt. Contact phenomena in the flange are taken into account, and by means of an incremental procedure it becomes possible to follow the development of these phenomena throughout the loading history. Material nonlinearity is also accounted for, both in the flange and the bolt, assuming a bilinear constitutive model. We propose several refinements of the model, which enhance its effectiveness with respect to intricate characteristics of T-stub behavior, such as bolt-flange interaction and three-dimensional geometry. The performance of the model is validated by comparison to experimental results found in the literature and by a parametric study performed in parallel with three-dimensional finite element analyses.

1. Introduction

Advanced analysis of steel structures requires extensive information regarding the behavior of both the members and the joints. For the members, well established methodologies exist to account for nonlinearities in response. However, for joints, a similar level of methods is not available to predict response characteristics, and in particular the moment-rotation curve. This shortcoming is mainly due to the complex nature of joints, which are assemblages of multiple parts. Material and geometrical nonlinearities, contact phenomena, geometrical complexity and multiple typologies which govern the behavior of joints are an obstacle towards a systematic, theoretical, yet pragmatic treatment of this subject. To subdivide the problem, one can identify joint components with simplified behavior, and then reproduce the total response as an assembly of the partial responses of the individual components. In this context, various mechanical spring assemblies have been proposed for stiffness and strength calculations [Huber and Tschemmernegg 1998; CEN 2003], while a similar process has been suggested for other characteristics, such as rotational capacity and full moment-rotation curve [Kuhlmann and Kuhnemund 2000; Beg et al. 2004]. Generally, components of tensile, compressive and shear deformability can be identified in structural joints. The tensile components of common bolted joints, which provide the major source of deformability, have the form of equivalent T-stub connections [Yee and Melchers 1986; Weynand et al. 1995; Shi et al. 1996], as shown in Figure 1a.

Numerous research works are dedicated to the analytical estimation of strength and stiffness of T-stub connections. [Zoetemeijer 1974; Agerskov 1976; Yee and Melchers 1986], among others, contributed to a basis for the currently established and codified T-stub model [CEN 2003]. Regarding the complete

The research in this paper is part of a project which is cofunded by the European Social Fund (75%) and National Resources (25%). This contribution is gratefully acknowledged.

Keywords: T-stub connection, T-stub model, steel connections, contact phenomena, nonlinearity.

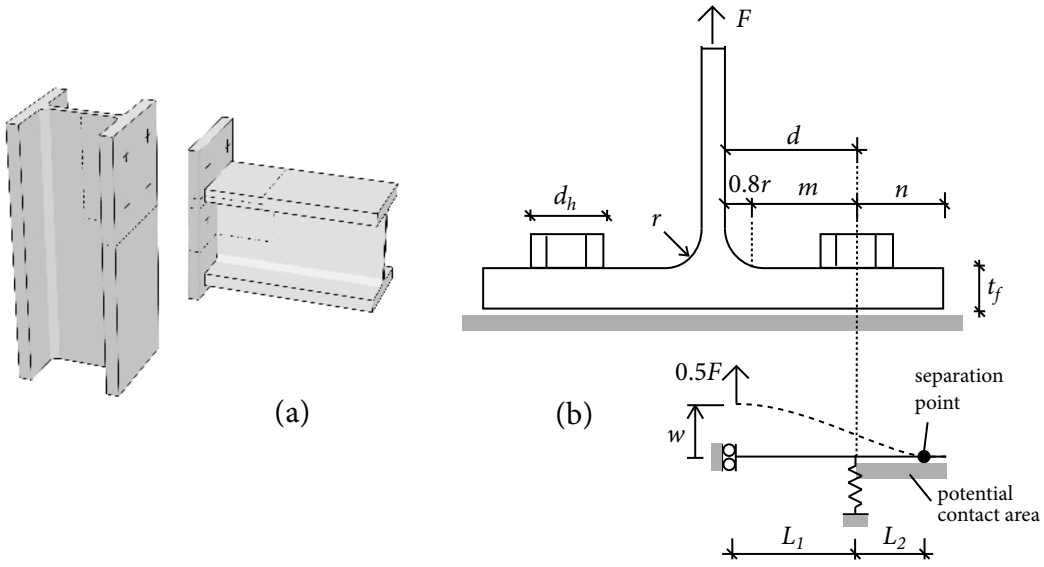

Figure 1. (a) T-stub components in a bolted beam-to-column joint and (b) T-stub definitions and the analytical model (b).

force-displacement curve, available methodologies include the bilinear model of [Jaspart 1991], the quadrilinear model of [Faella et al. 2000], the incremental model of [Swanson and Leon 2001] and the finite element beam model of [Girão Coelho et al. 2004]. An alternative approach for prediction of T-stub response is the advanced finite element modeling. Further contributions have been devoted to this subject which employ 2D plane elements [Mistakidis et al. 1997] or 3D brick elements [Sherbourne and Bahaari 1996; Bursi and Jaspart 1997; Wanzek and Gebbeken 1999]. The performance of such models is generally very good, since geometrical characteristics and nonlinearities are adequately modeled. However, the merit of these models for practical design purposes is limited, due to the special software requirements they pose, their high computational cost and the large amount of output data they produce.

In this paper we propose an incremental analytical model for the prediction of the complete force-displacement curve of the T-stub connection. The proposed model is designed for implmentation in a computer program rather than hand calculation and assumes the following as relevant objectives: credible results, ease of programming, and minimum dependency on special software. To achieve credible results, our model is designed for implementation in a computer program rather than hand calculation. Published methodologies for prediction of the whole force-displacement curve generally require computer implementation [Faella et al. 2000; Swanson and Leon 2001; Girão Coelho et al. 2004]. In fact, T-stub behavior is so complicated that implementing a simplified method suitable for hand calculation would unavoidably compromise the credibility of the model. This becomes an even greater problem for the whole joint, since multiple components must be analyzed.

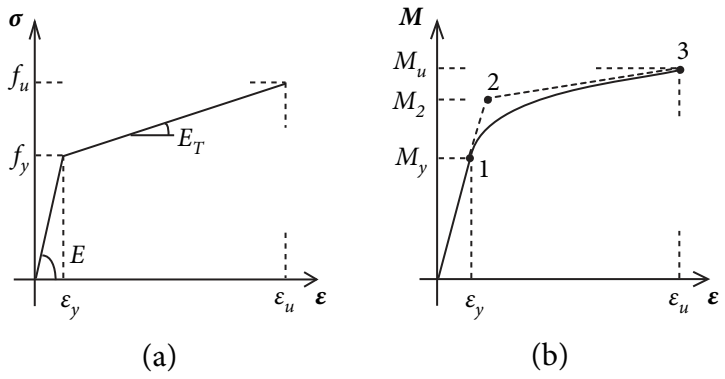

Figure 2. (a) Flange material modeling and (b) corresponding moment-outer fiber strain diagram.

2. Model description

T-stub connections are fairly complex to analyze. Their geometry is three-dimensional, and includes contact phenomena as well as interaction between the flanges and the bolts. Some compromises are taken into consideration to circumvent these difficulties. We first adopted a two-dimensional representation of the problem. This is opposed to the actual geometry which is three-dimensional due to the bolts and the holes at the flanges. As shown in Figure 1b, the analysis is based on classical beam theory, with the flanges modeled as beams and the bolts as springs of equivalent stiffness located at the axes of the physical bolts. Taking advantage of symmetry, we model only one half of the T-stub. The initially unknown distance of the flange edge, where the symmetry condition is enforced, from the bolt axis, is L_1. The area extending from the bolt spring to the free end is considered as potential contact area where partial separation might occur. The separation length measured from the bolt axis is L_2. Displacement w is identical to the vertical deflection of the flange mid-thickness at the symmetry plane which passes along the web.

2.1. ***Material nonlinearity.*** Both the flanges and the bolts feature a bilinear material law with strain hardening, shown in Figure 2a with E and E_T denoting the elasticity modulus and the hardening modulus respectively, ε_y, ε_u the yield and ultimate strain and f_y, f_u the yield and ultimate stress. Figure 2b shows the bending moment M – the outer fiber strain ε diagram for a rectangular cross section with this type of material. Point 1 of the diagram denotes the end of the elastic region, when the outer fibers of the cross section reach their yield strain ε_y. Beyond this point, and as larger parts of the cross section enter the plastic region, the curve gradually softens, up to the point of fracture, denoted by point 3 in the diagram.

It is assumed that fracture occurs when the outer fibers of the cross section reach their ultimate strain ε_u. Thus, the ultimate moment resistance can be expressed as

$$M_u = \frac{bt_f^2}{12}\left(3(E-E_T)\varepsilon_y + 2E_T\varepsilon_u - \frac{(E-E_T)\varepsilon_y^3}{\varepsilon_u^2}\right), \tag{1}$$

where b is the width of the flange, and the other symbols are shown in Figures 1b and 2a. When $\varepsilon_u \gg \varepsilon_y$, a hypothesis valid for steel, Equation (1) is simplified to become

$$M_u = \frac{bt_f^2}{12}(f_y + 2f_u). \tag{2}$$

We introduce an additional simplification regarding nonlinearity of the $M - \varepsilon$ curve. This curve is approximated by a bilinear representation, with the linear segments lying tangential to the original curve at points 1 and 3. The intersection of the two segments at point 2 in Figure 2b is proven to take place for a moment equal to

$$M_2 = \frac{bt_f^2}{4} f_y. \tag{3}$$

The bilinear simplification of the $M - \varepsilon$ curve allows one to distinguish the flange beam in parts where the bending moments have surpassed M_2 (and subsequently modulus E_T characterizes the material response), from the remaining parts, which remain elastic.

For the bolt, the bilinear material law results in a bilinear force versus elongation curve, since bolts are only subjected to tensile loading, so that calculation of the respective characteristics of the curve is straightforward.

2.2. ***Contact phenomena.*** A complex aspect of the T-stub behavior involves the contact of the flange surfaces. In existing methods [Jaspart 1991; Faella et al. 2000; Swanson and Leon 2001], the location of prying actions is predetermined and remains constant through the whole loading history. In our model, we make no assumption regarding the location of the prying actions. Instead, the part of the flange extending from the bolt location to the free end is considered as the potential contact area where partial separation might occur. A unique separation point appears somewhere within this area and the beam length beyond this point remains in complete contact with its base as shown in Figure 1b. Assuming that the base is infinitely rigid, this part of the beam remains straight, with zero curvature and, thus, zero moment. Due to continuity of the flange, the same conditions should apply locally to the separation point through the deformed part as well. Hence, both the rotation and the moment of the flange on both sides of the separation point should be zero. The calculation process takes advantage of these conditions to find the location of the separation point, as described later in this section.

The separation length L_2 changes during the loading progress, while additional parts of the flange or the bolt enter the plastic region, and we implement this behavior in the proposed incremental model. The conditions of zero moment and rotation apply throughout the response. Figure 3 shows the model used for the calculations, with the state of the total response in step i of the incremental process. The label A shows the edge near the web, located at a distance L_1 from the bolt axis, while B shows the bolt axis position, where the bolt spring is connected to the flange. Point C^i indicates the separation point at the current step i, with the current separation length L_2^i. Figure 3 also shows the incremental response between steps i and i+1, where the new separation point is indicated by C^{i+1} and the new separation length is L_2^{i+1}. For calculation of the new separation length L_2^{i+1}, a moment constraint is applied to the separation point C^{i+1} which allows for expression of the respective moment reaction as a function of the unknown L_2^{i+1}. However, as mentioned earlier, the separation point C^{i+1} must fulfill zero moment conditions. Therefore, we obtain an appropriate length L_2^{i+1} which causes the total moment to edge

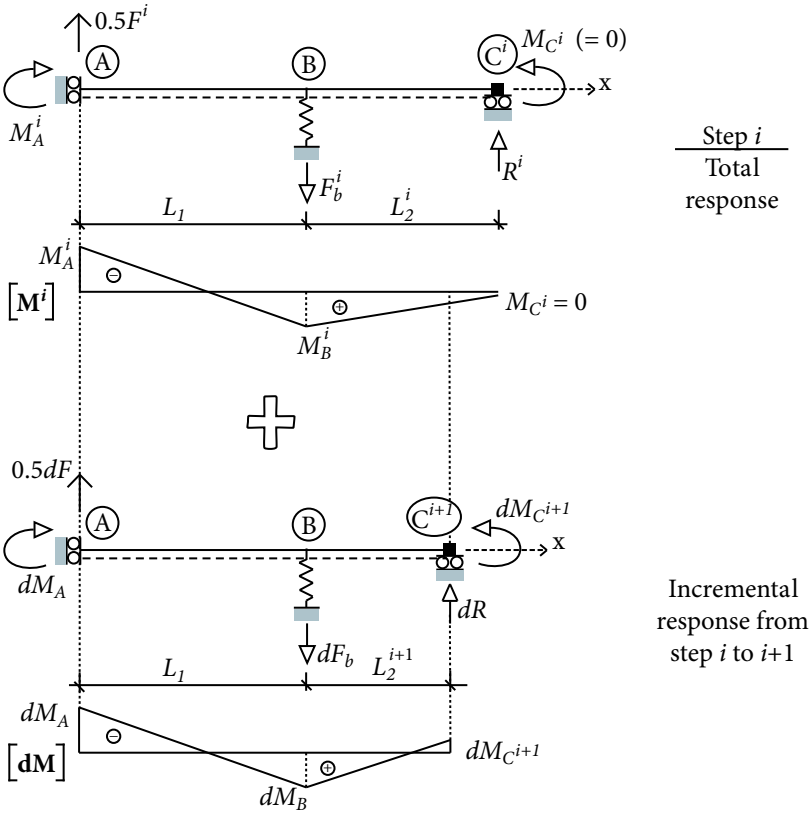

Figure 3. Incremental treatment of contact phenomena.

C^{i+1} to be zero. Note that the constraint symbol used in Figure 3 at the separation point represents a full moment support, but it differs from the conventional clamping symbol to signify the zero actual moment at this point. The enforcement of zero moment at the new separation point C^{i+1}, in the total response of step $i+1$, is given by

$$M_{C^{i+1}} = M^i(x = L_1 + L_2^{i+1}) + dM_{C^{i+1}} = 0 \Rightarrow \tag{4}$$

$$M_B^i L_2^i - M_B^i L_2^{i+1} + dM_{C^{i+1}} L_2^i = 0. \tag{5}$$

The total moment M_B^i is known from the previous step but the incremental moment $dM_{C^{i+1}}$ is a function of the new separation length L_2^{i+1}. Further elaboration of Equation (5) will be given in Section 2.4, where the required quantities of the response will be available analytically.

2.3. ***Flange length L_1.*** The modeled flange features a constant cross section. However, near the web, the real flange cross section gradually increases in height. The critical position for strength calculations, according to prEN 1993-1-8 [CEN 2003], lies at a distance $0.2r$ from the start of the flange-to-web fitting. However, using this length for stiffness calculations leads to overestimation of the response because the deformability of the remaining part of the fitting is ignored. Therefore, in our proposed model, we take

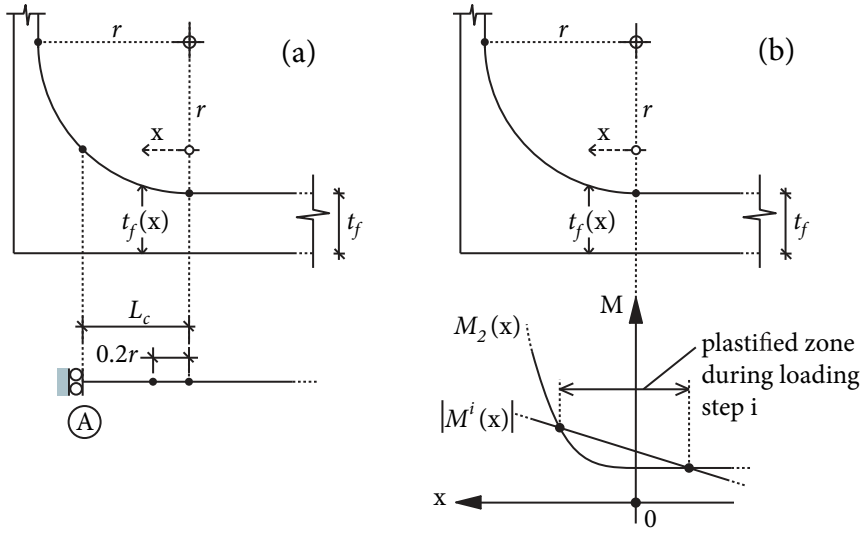

Figure 4. Approximation using the analytical model of (a) the flange-to-web fitting, and (b) definition of the plastified zone in the same region.

into account the total fitting length up to the web face. Because the real fitting has a variable cross section, an equivalent length L_c of constant cross section as shown in Figure 4a, is used so that the flexural stiffness of the two is equal as follows:

$$\int_0^r \frac{1}{EI(x)}\,dx = \int_0^{L_c} \frac{1}{EI}\,dx \Rightarrow \tag{6}$$

$$\int_0^r \frac{1}{(t_f(x))^3}\,dx = \int_0^{L_c} \frac{1}{t_f^3}\,dx. \tag{7}$$

The function $t_f(x)$ of the cross section height at a distance x from the start of the circular fitting, as shown in Figure 4a, is

$$t_f(x) = t_f + r - \sqrt{r^2 - x^2}. \tag{8}$$

The analytical integration of the left side of (7) is not readily available. Instead the trapezoidal rule can be applied as

$$\text{Int} = \int_0^r \frac{1}{t_f(x)^3}dx = \frac{r}{2k}\left(\frac{1}{t_f^3} + \frac{1}{(t_f + r)^3} + 2\sum_{j=1}^{k-1}\frac{1}{t_{f,j}^3}\right), \tag{9}$$

where $t_{f,j} = t_f\left(x = j\frac{r}{k}\right)$ and k the number of trapezoids to be used for the approximation. Typically, values of k equal to 4 or 5 provide sufficient accuracy. The equivalent fitting length should then be derived from (7) as

$$L_c = t_f^3\,\text{Int}\,. \tag{10}$$

Figure 4b illustrates the relevant process of obtaining the plastified flange zone at the flange-to-web fitting, which will be investigated in the following section.

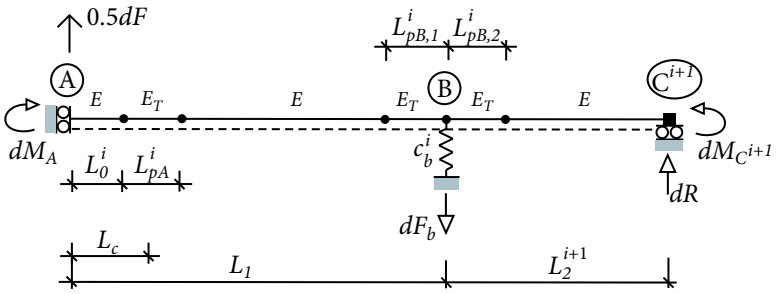

Figure 5. The proposed incremental model with all potential plastification zones in the flange.

2.4. ***Model response.*** The model is solved using the force method. As mentioned earlier, the incremental model features a moment constraint at C. Neglecting longitudinal forces, it is twice statically indeterminate. In Figure 5, the proposed incremental model is depicted in its more general form, with plastified parts in the flange-to-web fitting of length L^i_{pA} and at the bolt area of lengths $L^i_{pB,1}$, $L^i_{pB,2}$ where superscript i indicates the loading step. The resulting quantities of its response were obtained analytically and are summarized in Table 1. From this table, the incremental prying force dR, bolt force dF_b as well as moments $dM_{C^{i+1}}$, dM_A and dM_B, which correspond to points C^{i+1}, A and B respectively, can be calculated for a given value of the applied incremental force dF. Then, the incremental displacement dw of the T-stub can be calculated from the partial displacements $dw_{j=0\cdots2}$. Section 4.3 provides details regarding the displacement dw_s. No special physical meaning is attributed to the parameters $s_{j=0\cdots2}$, $p_{j=0\cdots3}$, $q_{j=0\cdots4}$, G_1, G_2 and λ listed in Table 1. These parameters are used to calculate the aforementioned incremental quantities of the model response, to reduce the complexity of the algebraic expressions.

Purely elastic response as well as special cases such as plastification near the flange-to-web fitting can be derived from the expressions of Table 1 by substituting the respective plastification lengths with zero. This facilitates implementation of the model in computer code by avoiding multiple programming paths.

The plastification length L^i_{pA} is not adjacent to A but allows for a flange length L^i_0 to remain elastic. This compensates for its increased moment resistance. The exact value of length L^i_{pA} and its position is obtained by solving

$$|M^i(x)| = M_2(x), \tag{11}$$

where $M^i(x)$, the total bending moment in the flange during loading step i at distance x from the start of the fitting, is defined as

$$M^i(x) = M^i_A + 0.5F^i(L_c - x). \tag{12}$$

The moment resistance $M_2(x)$ is calculated from Equation (3), where instead of the constant cross section height t_f, we use

$$t_f(x) = \begin{cases} t_f + r - \sqrt{r^2 - x^2}, & x > 0, \\ t_f, & x \le 0. \end{cases} \tag{13}$$

If plastification occurs, solution of Equation (11) provides two roots as shown in Figure 4b for the definition of the length L^i_{pA}. Because part of the distance between the two roots obtained by (11) is located at the flange-to-web fitting, where the flange height is variable, a correction similar to the one

$$dR = \frac{3dF}{2}\frac{s_2(L_2^{i+1})^2 + s_1 L_2^{i+1} + s_0}{q_4(L_2^{i+1})^4 + q_3(L_2^{i+1})^3 + q_2(L_2^{i+1})^2 + q_1 L_2^{i+1} + q_0}$$

$$dM_{C^{i+1}} = -\frac{dF}{2}\frac{p_3(L_2^{i+1})^3 + p_2(L_2^{i+1})^2 + p_1 L_2^{i+1} + p_0}{q_4(L_2^{i+1})^4 + q_3(L_2^{i+1})^3 + q_2(L_2^{i+1})^2 + q_1 L_2^{i+1} + q_0}$$

$$dF_b = \frac{dF}{2} + dR$$

$$dM_A = -\frac{dF}{2}L_1 + dRL_2^{i+1} + dM_{C^{i+1}}, \qquad dM_B = dRL_2^{i+1} + dM_{C^{i+1}}$$

$$dw = dw_0 + dRdw_1 + dM_{C^{i+1}}dw_2\big(+dw_s\big)$$

$$dw_0 = \frac{dF}{6EI}\left(L_1^3 + \lambda\Big(\big(L_{pA}^i\big)^3 + \big(L_{pB,1}^i\big)^3 + 3L_{pA}^i\big(L_1 - L_0^i\big)\big(L_1 - L_0^i - L_{pA}^i\big)\Big) + \frac{3EI}{c_b^i}\right)$$

$$dw_1 = -\frac{1}{2EI}\left(L_1^2 L_2^{i+1} + \lambda L_2^{i+1}G_1 - \frac{2EI}{c_b^i}\right), \qquad dw_2 = -\frac{1}{2EI}\left(L_1^2 + \lambda G_1\right), \qquad dw_s = 0.5\,\frac{dFL_1}{GA}$$

$$s_2 = c_b^i\big(L_1^2 + \lambda G_1\big)$$
$$s_1 = -4EI$$
$$s_0 = -4EI\big(L_1 + \lambda G_2\big) + c_b^i\lambda\big(L_{pB,2}^i\big)^2\big(L_1^2 + \lambda G_1\big)$$

$$p_3 = c_b^i\big(L_1^2 + \lambda G_1\big)$$
$$p_2 = -6EI$$
$$p_1 = -12EI\big(L_1 + \lambda G_2\big) + 3c_b^i\lambda\big(L_{pB,2}^i\big)^2\big(L_1^2 + \lambda G_1\big)$$
$$p_0 = -6EI\big(L_1^2 + \lambda\big(G_1 - \big(L_{pB,2}^i\big)^2\big)\big) - 2c_b^i\lambda\big(L_{pB,2}^i\big)^3\big(L_1^2 + \lambda G_1\big)$$

$$q_4 = c_b^i$$
$$q_3 = 4c_b^i\big(L_1 + \lambda G_2\big)$$
$$q_2 = -6c_b^i\lambda\big(L_{pB,2}^i\big)^2$$
$$q_1 = 12EI + 4c_b^i\lambda\big(L_{pB,2}^i\big)^3$$
$$q_0 = 12EI\big(L_1 + \lambda G_2\big) + 4c_b^i\lambda\big(L_{pB,2}^i\big)^3\Big(L_1 + \lambda\Big(G_2 - \frac{3L_{pB,2}^i}{4}\Big)\Big)$$

$$G_1 = 2\big(L_1 - L_0^i\big)L_{pA}^i + \big(L_{pB,1}^i\big)^2 - \big(L_{pA}^i\big)^2$$
$$G_2 = L_{pA}^i + L_{pB,1}^i + L_{pB,2}^i \qquad \lambda = \frac{E - E_T}{E_T}$$

Table 1. Analytical expressions for the incremental response from step i to $i+1$.

mentioned in Section 2.3 is required, to correspond to the constant cross section height t_f used for the flange in the model. The only difference is in the computation of the integral in Equation (9), in which the minimum of two roots should be used as lower boundary and the maximum one as upper boundary.

A similar procedure can be used for determining the plastified lengths $L^i_{pB,1}$ and $L^i_{pB,2}$. In this case however, the flange cross section remains constant, so the computations for the two lengths are more straightforward.

Substituting $dM_{C^{i+1}}$ from Table 1 into Equation Equation (5), the separation length L_2^{i+1} in the new step can be calculated from the following fifth order polynomial equation:

$$m_5(L_2^{i+1})^5 + m_4(L_2^{i+1})^4 + m_3(L_2^{i+1})^3 + m_2(L_2^{i+1})^2 + m_1 L_2^{i+1} + m_0 = 0, \tag{14}$$

where the factors $m_{j=0\cdots5}$ are:

$$\begin{aligned}
m_5 &= -M_B^i q_4 \\
m_4 &= M_B^i L_2^i q_4 - M_B^i q_3 \\
m_3 &= M_B^i L_2^i q_3 - M_B^i q_2 - 0.5 dF L_2^i p_3 \\
m_2 &= M_B^i L_2^i q_2 - M_B^i q_1 - 0.5 dF L_2^i p_2 \\
m_1 &= M_B^i L_2^i q_1 - M_B^i q_0 - 0.5 dF L_2^i p_1 \\
m_0 &= M_B^i L_2^i q_0 - 0.5 dF L_2^i p_0
\end{aligned} \tag{15}$$

and the factors $q_{j=0\cdots4}$, $p_{j=0\cdots3}$ are the same as in Table 1.

Equation (14) is best solved using a Newton–Raphson scheme since the derivative is easily available. If the obtained solution from (14) exceeds the physical length n of the T-stub, then no partial contact occurs in the flange and instead a simple support at the flange edge should be applied. In that case, the incremental model is once statically indeterminate and its response differs from the one given in Table 1. The required quantities of the response, with simple support conditions at the flange edge are presented in Table 2. For a given value of the applied incremental force dF, we calculate the incremental forces dR and dF_b, moments, dM_A and dM_B, and subsequently, from the same table, the incremental displacement dw. As with Table 1, no special physical meaning is attributed to the parameters $s_{j=0\cdots1}$, $q_{j=0\cdots3}$, G_1, G_2 and λ. Length L_2^{i+1} in Table 2 is equal to distance n from bolt axis to flange edge. However, the notation is retained for reasons of uniformity and continuity of the expressions.

Once simple support conditions apply to the edge, the flange rotation φ_C at this location becomes nonzero. The occurrence of partial contact again, at a later load increment, for example in case of subsequent plastification in the flange, should be allowed only after the negation of this previously accumulated rotation φ_C, together with a solution of (14) for a length L_2^{i+1} less than the physical length n.

3. Solution process

The objective of the solution process is to generate the load F vs. displacement w curve. The scheme of the incremental process is shown in Figure 6. At each cycle of the process, an incremental loading is determined and the incremental response and the new separation length are calculated. Then, the incremental response of the current load increment is appended to the last total response. At this point the

$$dR = \frac{3dF}{4}\,\frac{s_1 L_2^{i+1} + s_0}{q_3 (L_2^{i+1})^3 + q_2 (L_2^{i+1})^2 + q_1 L_2^{i+1} + q_0}$$
$$dF_b = \frac{dF}{2} + dR$$
$$dM_A = -\frac{dF}{2} L_1 + dR L_2^{i+1}, \qquad dM_B = dR L_2^{i+1}$$

$$dw = dw_0 + dR\,dw_1 \big(+dw_s\big)$$
$$dw_0 = \frac{dF}{6EI}\left(L_1^3 + \lambda\Big(\big(L_{pA}^i\big)^3 + \big(L_{pB,1}^i\big)^3 + 3L_{pA}^i\big(L_1 - L_0^i\big)\big(L_1 - L_0^i - L_{pA}^i\big)\Big) + \frac{3EI}{c_b^i}\right)$$
$$dw_1 = -\frac{1}{2EI}\left(L_1^2 L_2^{i+1} + \lambda L_2^{i+1} G_1 - \frac{2EI}{c_b^i}\right)$$
$$dw_s = 0.5\,\frac{dF L_1}{GA}$$

$$s_1 = c_b^i\big(L_1^2 + \lambda G_1\big)$$
$$s_0 = -2EI$$
$$q_3 = c_b^i$$
$$q_2 = 3c_b^i\big(L_1 + \lambda G_2\big)$$
$$q_1 = -3c_b^i \lambda \big(L_{pB,2}^i\big)^2$$
$$q_0 = 3EI + c_b^i \lambda \big(L_{pB,2}^i\big)^3$$
$$G_1 = 2\big(L_1 - L_0^i\big)L_{pA}^i + \big(L_{pB,1}^i\big)^2 - \big(L_{pA}^i\big)^2$$
$$G_2 = L_{pA}^i + L_{pB,1}^i + L_{pB,2}^i \qquad \lambda = \frac{E - E_T}{E_T}$$
$$L_2^{i+1} = \text{the distance } n \text{ from bolt axis to flange edge}$$

Table 2. Analytical expressions for the incremental response with simple support conditions at the flange edge from step i to $i+1$.

total bending moments of the flange and the total bolt force are known and therefore decisions regarding the plastification or failure of flange regions or the bolt can be made. The new flange plastification lengths and the bolt stiffness are computed before a new cycle starts. The process continues until failure is detected either in the flange or in the bolt.

4. Model refinements

4.1. ***Bolt head size.*** In real T-stubs, the bolt acts on the flange through its head within an extended region of contact between flange and bolt head. However, in our model bolt action is concentrated at a

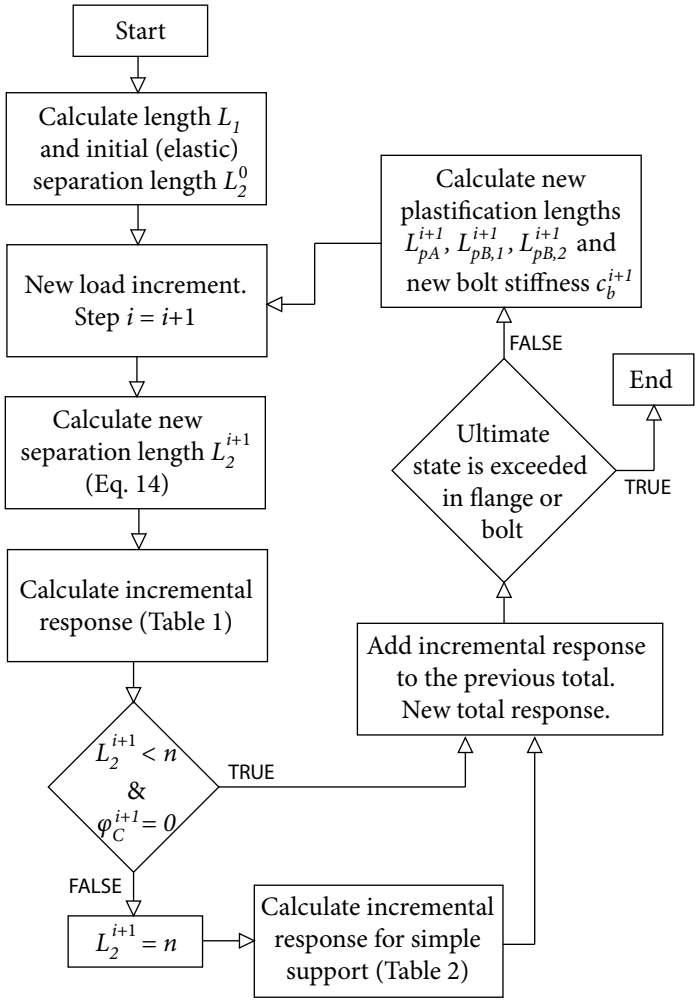

Figure 6. Solution process.

single point of the flange. As shown in Figure 7a, the solution derived from a concentrated bolt action overestimates the flange bending moment at the bolt location. Assuming a uniform distribution of the bolt force within a zone of length equal to the bolt head diameter d_h, the variation of the moment at the bolt location, compared to the case of concentrated action, is given by

$$\Delta M_B = \frac{F_b d_h}{8}. \tag{16}$$

This variation is taken into account when a decision regarding plastification or failure of the flange at the bolt location is taken.

Note that no special consideration made of the influence of the hole and the reduced cross section of the flange on the moment capacity of the flange. In theory, the beneficial action of the uniform distribution of the bolt force could be compensated by the unfavorable effect of the reduced flange cross

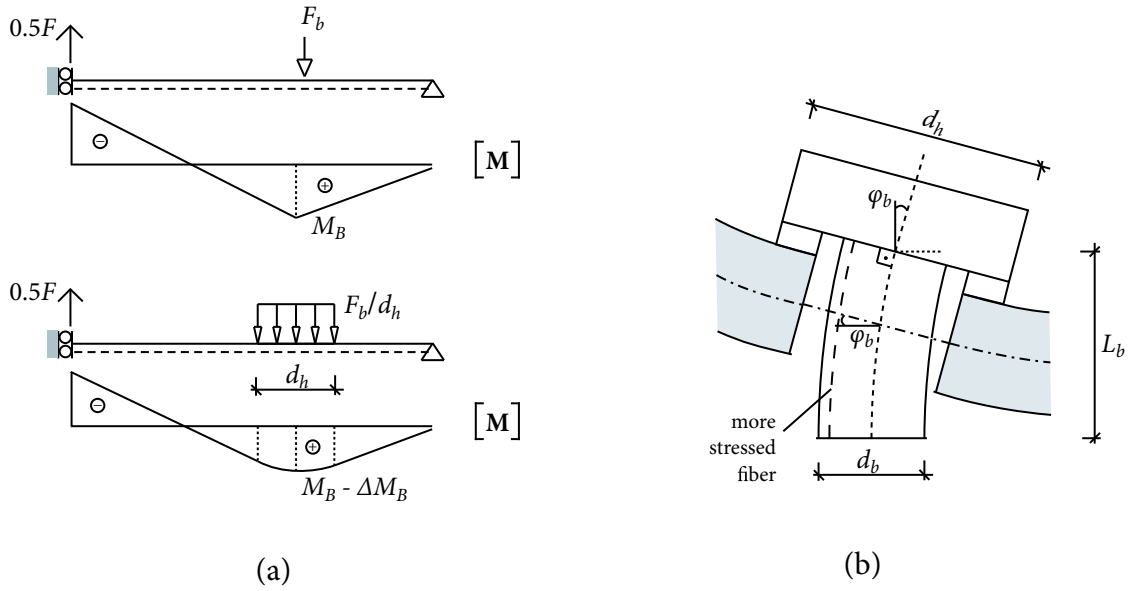

Figure 7. Influence of bolt head size (a) and definitions for the bolt bending treatment (b).

section. However, the behavior of the flange in the area near the bolt departs from simple bending, it is characterized by a complex three dimensional stress state, and it is affected by the interaction with the bolt head. Designation of a reduced moment capacity for the flange at the bolt area, based on its net cross section, lead to significant underestimate of the strength of the complete T-stub. Therefore, we do not propose such reduction to the flange moment capacity.

4.2. ***Bolt bending.*** The bolt shank of a real T-stub is subjected to combined tension and bending, whereas in the proposed model only axial tension is considered. This potentially leads to a considerable overestimation of the maximum axial load the bolt can carry. In T-stubs with strong flanges where the bolts are critical for the ultimate load capacity, a slight overestimation of the bolt resistance can lead to significant overestimation of the ultimate T-stub displacement.

To prevent this error we assume a revised criterion for the realization of the ultimate bolt state, which refers to the more stressed fiber of the bolt shank shown in Figure 7b, as

$$\varepsilon_u > \varepsilon_t + \varepsilon_b, \tag{17}$$

where ε_u is the ultimate strain of the bolt material, ε_t the strain attributed to tensile action and ε_b the strain attributed to bending action. The value of ε_t can be obtained from

$$\varepsilon_t = \frac{w_b}{L_b}, \tag{18}$$

where L_b is the modeled shank length and w_b the elongation of the bolt shank, which can be calculated throughout the incremental process using the current bolt stiffness and the incremental axial bolt force dF_b. For ε_b, we assume that the total rotation of the bolt shank axis φ_b, is equal to the flange rotation at this position (Figure 7b) available analytically at each incremental step. Because the bending of the

shank is induced through rotation of its edges, constant bending moments along its length is assumed, and thus strain ε_b is related to rotation φ_b through

$$\varepsilon_b = \frac{d_b/2}{L_b}\,\varphi_b. \tag{19}$$

Note that for wide T-stubs the deformation of the flange is not uniform along its width. Near the bolts the flange deflection and rotation is reduced compared to a uniform deformation, as assumed in the model. In such cases the criterion in Equation (17) can lead to early failure. We tested our proposed model for T-stub configurations with b/m ratios up to $2.0 \sim 2.5$, and obtained acceptable results, as shown in the following sections. For even wider T-stubs, further study is necessary to make a meaningful estimation of the bolt rotation.

4.3. ***Shear deformations.*** The expressions in Tables 1 and 2 account for the work in the flange due to bending actions only. This assumption is normally valid for long beams where work due to shear deformation may be neglected. For T-stubs, the dimensions of the flanges do not justify this simplification. Expressions similar to the ones in Tables 1 and 2 can be derived with the shear work included. However, such expressions are more complicated and are not presented in this paper. Instead, a simple circumvention is possible, in which we account for the shear work in the calculations of the resulting displacements only. Thus, the following quantity may be added to the displacements dw in Tables 1 and 2:

$$dw_s = \int_0^{L_1} \frac{0.5dF \cdot \bar{1}}{GA}\,dx = \frac{dFL_1}{2GA}. \tag{20}$$

4.4. ***Three-dimensional stress and strain state.*** In our model the flange is treated as a simple Bernoulli beam. Hence, any secondary stresses are neglected, such as the normal σ_{yy} and σ_{zz} with y and z axes as defined in Figure 8. However, this assumption for the stress state is accurate enough only near the two side edges and for fairly thin flanges. Towards the middle areas of the width b, lateral strain ε_{zz} is suppressed, resembling plane strain conditions. Assuming that $\varepsilon_{zz} = 0$ and that σ_{yy} also remains practically zero due

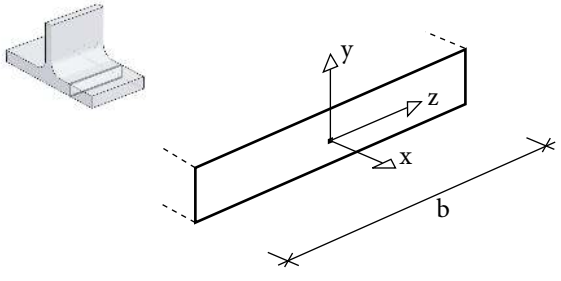

Figure 8. Flange cross sectional axis definitions.

to the flange being adequately thin, the three dimensional elastic stress-strain equations lead to

$$\sigma_{xx} = \frac{E}{1-v^2}\,\varepsilon_{xx}, \tag{21}$$

$$\sigma_{zz} = \frac{\nu E}{1-v^2}\,\varepsilon_{xx}. \tag{22}$$

Equation (21) suggests adoption of an equivalent modulus of elasticity for the flange

$$E^* = \frac{E}{1-\nu^2}. \tag{23}$$

For Poisson's ratio ν equal to 0.3, an equivalent modulus E^* becomes approximately 10% larger than E. The interaction of normal stress σ_{xx} and the nonzero secondary σ_{zz} applied in the von Mises yield criterion leads to an equivalent yield stress:

$$f_y^* = \frac{f_y}{\sqrt{1-v+\nu^2}}. \tag{24}$$

For $\nu = 0.3$, (24) leads to an approximately 13% increase of the equivalent yield stress of the flange.

To determine an equivalent modulus E_T^* in the plastic region, we adopt the deformation theory of plasticity [Chen and Han 1988], which implies a proportional loading history. The plastic strains are a function of the total stresses

$$\varepsilon_{xx}^p = \frac{\varepsilon_{\text{eff}}^p}{\sigma_{\text{eff}}}\left(\sigma_{xx} - \tfrac{1}{2}(\sigma_{yy}+\sigma_{zz})\right), \tag{25}$$

$$\varepsilon_{yy}^p = \frac{\varepsilon_{\text{eff}}^p}{\sigma_{\text{eff}}}\left(\sigma_{yy} - \tfrac{1}{2}(\sigma_{xx}+\sigma_{zz})\right), \tag{26}$$

$$\varepsilon_{zz}^p = \frac{\varepsilon_{\text{eff}}^p}{\sigma_{\text{eff}}}\left(\sigma_{zz} - \tfrac{1}{2}(\sigma_{xx}+\sigma_{yy})\right), \tag{27}$$

where $\varepsilon_{\text{eff}}^p$ and σ_{eff} are the effective plastic strain and the effective stress, respectively. Imposing $\varepsilon_{zz} = 0$ and $\sigma_{yy} = 0$, the nonzero plastic strains are

$$\varepsilon_{xx}^p = \frac{3}{4}\,\frac{\varepsilon_{\text{eff}}^p}{\sigma_{\text{eff}}}\sigma_{xx}, \tag{28}$$

$$\varepsilon_{yy}^p = -\frac{3}{4}\,\frac{\varepsilon_{\text{eff}}^p}{\sigma_{\text{eff}}}\sigma_{xx}, \tag{29}$$

while for the nonzero total normal stresses

$$\sigma_{zz} = \frac{1}{2}\,\sigma_{xx}. \tag{30}$$

The equivalent ultimate stress can be derived from (30) using the von Mises criterion

$$f_u^* = \frac{2\sqrt{3}}{3}\,f_u. \tag{31}$$

Finally, the equivalent modulus E_T^* can be defined as the slope of the line in the stress-strain plane leading from the equivalent yield state to the equivalent ultimate state

$$E_T^* = \frac{f_u^* - f_y^*}{\varepsilon_{xx,u} - \varepsilon_{xx,y}}, \tag{32}$$

where $\varepsilon_{xx,y}$ is the yielding strain obtained from (21) and $\varepsilon_{xx,u}$ is the ultimate strain obtained from (21) and (28) as

$$\varepsilon_{xx,u} = \frac{2\sqrt{3}}{3}\,\frac{f_u}{E}\,(1-\nu^2) + \frac{\sqrt{3}}{2}\,(f_u - f_y)\,\frac{E - E_T}{E\,E_T}. \tag{33}$$

4.5. ***Flange-bolt interaction.*** In our proposed model, we assume a uniform flange deflection along its width b. However, in real T-stubs, especially wide ones, this assumption is not appropriate due to the bolt action which is exerted in a part only of the total width. This discrepancy affects the calculated displacements of the analytical model. Using an equivalent plate problem, [Faella et al. 2000] proposed a modified effective width b_{eff} for stiffness calculations. The plate features an infinite width which mainly applies to T-stubs which are considered as components of more complex connections where the dimensions of the plates are quite large compared to the individual T-stubs. Under these assumptions, b_{eff} is simply derived as

$$b_{\text{eff}} = 2.21m. \tag{34}$$

The length m is shown in Figure 1b and is equal to $d - 0.8r$. For completeness of the proposed model, we undertook a similar approach for plates of finite width. In particular, cantilevered plates with varying values of m/b loaded with a concentrated load in the middle of the free edge, opposite to the clamped one, were analyzed elastically using 2D plate finite elements. Comparing the numerically calculated displacements of the plates to those of a simple beam representation, for an equivalent width b_{eff}, we obtained

$$\frac{b}{b_{\text{eff}}} = \begin{cases} 0.92 + \frac{0.06}{(m/b)^2}, & m/b < 0.87, \\ 1, & m/b \geq 0.87. \end{cases} \tag{35}$$

Figure 9 shows a graphical representation of Equation (35) as well as the curve derived from Equation (34) from [Faella et al. 2000]. Considering that Equation (34) is based on an analysis of infinitely wide plates, it is expected that for low values of the ratio m/b, the two curves converge. However, for intermediate values of the ratio m/b, we observe a difference up to 20% in the equivalent width b_{eff}.

This equivalent width b_{eff} is used to calculate the resulting displacements due to flange deformation only. Decoupling of the total T-stub displacement w, which is calculated incrementally by means of Table 1 or 2, to flange and bolt contributions, can be performed at each incremental step since the bolt elongation is easily obtainable using the current bolt stiffness and the incremental axial force dF_b. The decoupled flange deflection should then be corrected with the multiplier b/b_{eff} from Equation (35), to better approximate the impact of three-dimensional flange deformation.

5. Model performance

5.1. ***Comparison with experimental tests.*** Performance of our proposed model is validated by comparison with results of published experimental tests, as well as by numerical parametric analyses. The

published tests we used are those for T-stubs T1 and T2 conducted by [Bursi and Jaspart 1997], for which all the necessary geometrical properties are provided in Table 3. T-stub T1 features a relatively weak flange which is critical for the response, unlike T-stub T2 which features a stronger flange in which both the bolts and the flange are critical for the response. With reference to prEN 1993-1-8 [CEN 2003], those two behaviors correspond to the first and second failure mode, respectively. The bilinear material approximations applied for the incremental models are shown in Figure 10a and 10b. Engineering values are adopted since the original undeformed geometrical formulation is used for the calculations. Web material data are needed because in the experimental setup the displacements were measured at the web. The web deformability can be easily included in our model through an axially loaded spring of equivalent stiffness.

In Figures 11a and 11b, the force F vs. displacement w curves for the proposed analytical model and the experimental tests T1 and T2 are presented. Also, the curves derived by means of 3D finite element simulation performed with ADINA v.8 [ADINA 2004], as described later in section 5.2, are included in the same figure. For the finite element analyses, the ultimate state is realized when the von Mises stress in the critical regions of the flange or at the bolt shank approaches the respective material ultimate value. Likewise, for our proposed model, the ultimate state is realized when flange moments reach the ultimate moment M_u or when the criterion (17) regarding combined tension and bending of the bolt is violated.

The performance of the proposed model is shown to be quite satisfactory. For T-stub T1 initial stiffness, ultimate load, ultimate displacement and the overall curve converge to their experimental counterparts. The knee range is sharper in the proposed model as well as in the 3D finite element model. We

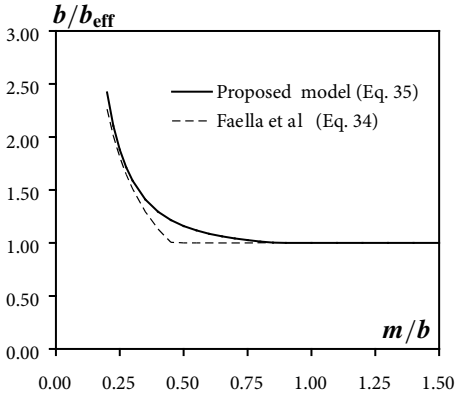

Figure 9. Curves for the estimation of the equivalent width b_{eff}.

	Flange					Bolt		
	b	t_f	r	d	n	d_b	d_h	L_b
T1	40.0	10.7	15.0	41.45	30.0	12.0	24.0	14.0
T2	40.0	16.0	18.0	40.25	30.0	12.0	24.0	16.0

Table 3. Geometrical characteristics for T-stubs in the parametric study (in mm).

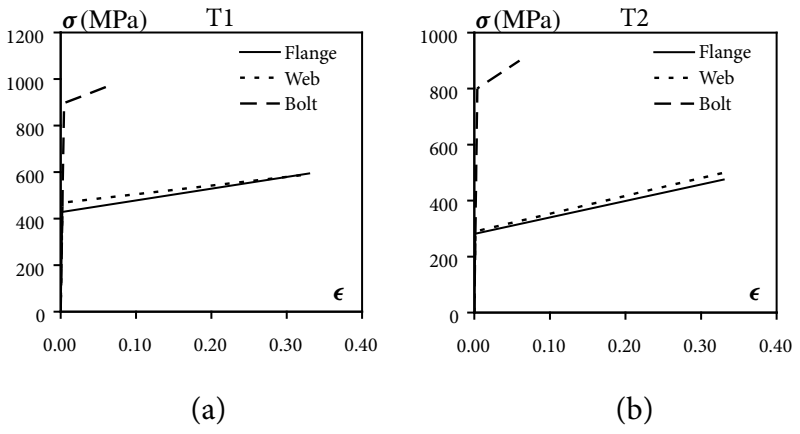

Figure 10. Bilinear material approximations for T-stubs (a) T1 and (b) T2.

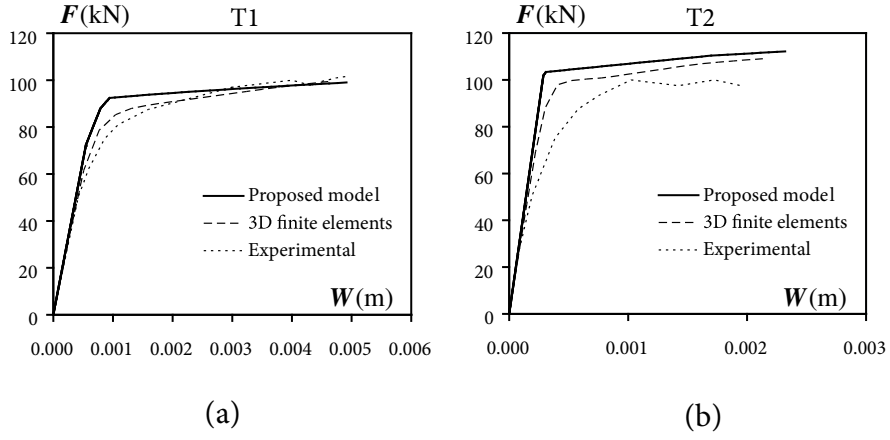

Figure 11. Force-displacement curves for T-stubs (a) T1 and (b) T2.

attribute this mainly to the bilinear approximation of the moment-curvature relationship for the flange and to the residual stresses present in the experimental flange. For T-stub T2, [Bursi and Jaspart 1997] mention that bolt thread stripping was observed and the experimental curve reflects this special failure type. Nevertheless, the curve of the proposed model lies fairly close to the 3D finite element one, for which thread detailing is also not modeled. A slight overestimation in the plastic branch can be observed. This is a result of the bolt bending action, which apart from the ultimate state, is neglected in the proposed model.

For flange contact, our proposed model for T-stub T2 reproduces simple support conditions at the flange edge which is validated by the finite element model and the physical test. For T-stub T1 the variation of the separation length L_2 through the loading history for the proposed model is shown in Figure 12a. After the first plastification in the flange area near the web, the separation length decreases

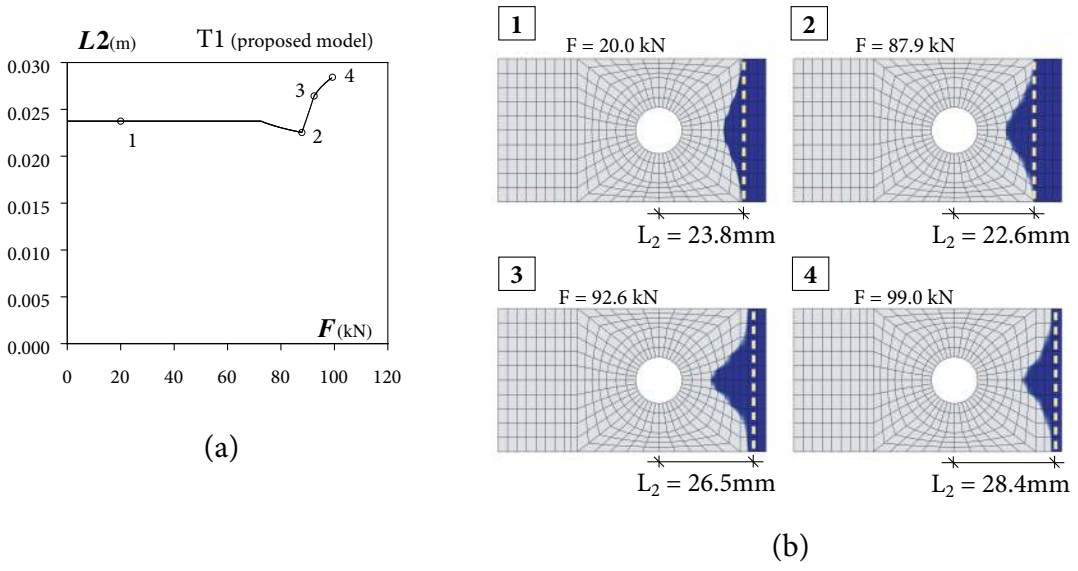

Figure 12. Development of flange contact phenomena in the proposed model (a) and in 3D finite element model (shown in dark shaded area) (b) for *T*-stub T1.

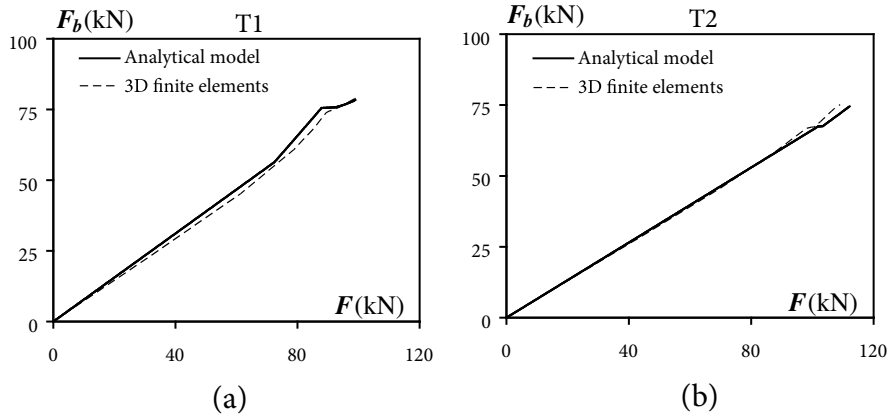

Figure 13. Bolt force versus external loading for *T*-stubs (a) T1 and (b) T2.

initially, but later when the bolt enters the plastic region, it increases. This behavior is confirmed by the results obtained by 3D finite element analysis shown in Figure 12b, where the contact area of the flange is plotted for various load levels. Note that the limits of the contact area provided by our model for the same loading levels are indicated with dashed lines.

In Figure 13, the axial force history for the bolt given by our model is compared to the 3D finite element results for both tests. The proposed model appears to perform very well in this context, especially considering the simplified method for including the bolt contribution, as compared to the more complex finite element method.

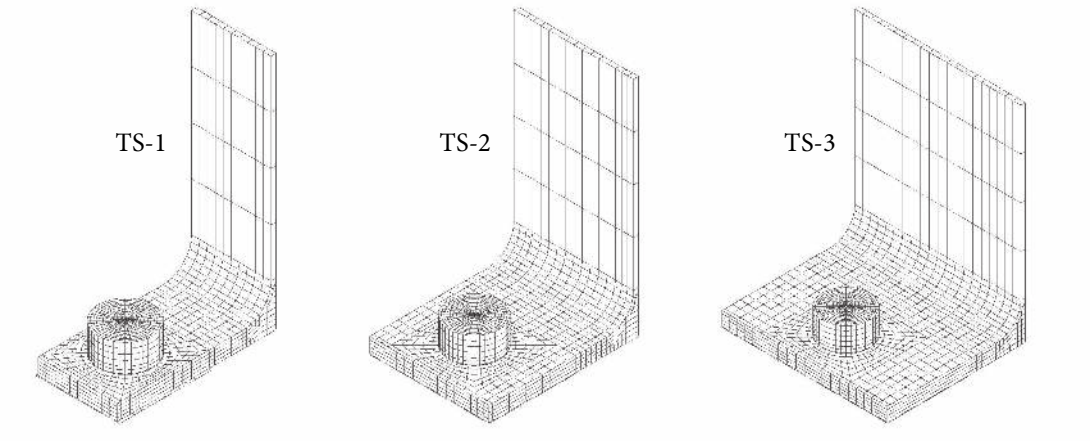

Figure 14. Typical finite element models for the parametric study.

5.2. ***Comparison through parametric finite element modeling.*** We also carried out a parametric study of the performance of our proposed model employing 3D finite element modeling with the software package ADINA v.8 [ADINA 2004]. The reliability of 3D finite element modeling for the T-stub connection has been confirmed in [Bursi and Jaspart 1997; Wanzek and Gebbeken 1999; Gantes and Lemonis 2003]. We validate its reliability here as well, through the comparison with the experimental tests T1 and T2 mentioned earlier. The flange and the bolts were modeled as separate bodies by means of eight node brick elements. The contact between them was modeled through 2D contact elements, equipped with constraint functions to enforce all contact conditions to the corresponding surfaces and a Coulomb friction coefficient equal to 0.25. In contrast, frictionless contact conditions were applied between the flange and its base which constitutes a symmetry plane of the whole problem. Through the thickness of the flange, five brick elements were employed, formulated with incompatible modes in order to circumvent the shear locking effect. Likewise, for the bolt circumference we implemented a large number of elements (40 or more). The loading was applied by prescribed displacements on the upper surface of the web with assumptions of large strains and large displacements globally imposed. Figure 14 shows the finite element plots for three of the models of the parametric study.

Table 4 lists the geometric properties of the T-stubs of the parametric study, while Table 5 lists the material properties, which remain unchanged for all T-stubs. The geometrical configurations in the parametric study include T-stubs with wide range of flange width and of relative strength between flange and bolts. The former allows investigation of the influence of the T-stub width to the flange-bolt interaction. We can also demonstrate the impact of the adopted beam representation in the ability of the model and its refinements to predict accurately the response of the three-dimensional problem.

Figure 15 shows the plots of force F against displacement w for the proposed analytical and the corresponding finite element models of the parametric study. In all cases the analytical curve closely matches the numerical one. The characteristic attributes of initial stiffness, ultimate strength and ultimate displacement are predicted within a fairly narrow margin of error. Performance is better for strength estimation than for initial stiffness and ultimate displacement. For the ultimate displacement, which is the most difficult characteristic to compute analytically, the maximum error does not exceed 30% for any

	Flange					Bolt		
	b	t_f	r	d	n	d_b	d_h	L_b
TS-1	50.0	10.0	18.0	66.75	30.0	20.0	34.0	14.0
TS-2	80.0	10.0	18.0	66.75	30.0	20.0	34.0	14.0
TS-3	120.0	10.0	18.0	66.75	30.0	20.0	34.0	14.0
TS-4	50.0	10.0	18.0	66.75	30.0	12.0	24.0	13.0
TS-5	80.0	10.0	18.0	66.75	30.0	12.0	24.0	13.0
TS-6	120.0	10.0	18.0	66.75	30.0	12.0	24.0	13.0
TS-7	50.0	15.0	18.0	65.50	30.0	20.0	34.0	19.0
TS-8	80.0	15.0	18.0	65.50	30.0	20.0	34.0	19.0
TS-9	120.0	15.0	18.0	65.50	30.0	20.0	34.0	19.0
TS-10	50.0	15.0	18.0	65.50	30.0	12.0	24.0	18.0
TS-11	80.0	15.0	18.0	65.50	30.0	12.0	24.0	18.0
TS-12	120.0	15.0	18.0	65.50	30.0	12.0	24.0	18.0

Table 4. Geometrical characteristics for T-stubs in the parametric study (in mm).

of the T-stubs and is much lower for most of them. Table 6 presents the mean value and the standard deviation of the relative errors in the parametric study for the three characteristic properties. A slight overestimation of the initial stiffness can be noticed from the results, while for the ultimate strength and displacement the mean error is very close to zero. Also, the low value of error standard deviation, observed for all three properties, indicates a consistent performance of the proposed model.

6. Conclusion

A new incremental T-stub model for the prediction of the complete force vs. displacement curve has been introduced in this paper. The model is designed for implementation in a computer program, and

	E	E_T	f_y	f_u
Flange	200000	782	355	510
Bolt	200000	2400	640	800

Table 5. Material properties for T-stubs in the parametric study (in MPa).

	Initial stiffness error	Strength error	Ultimate displacement error
Mean value	0.17	−0.02	0.03
Standard deviation	0.103	0.025	0.147

Table 6. Relative errors for the proposed model in the parametric study.

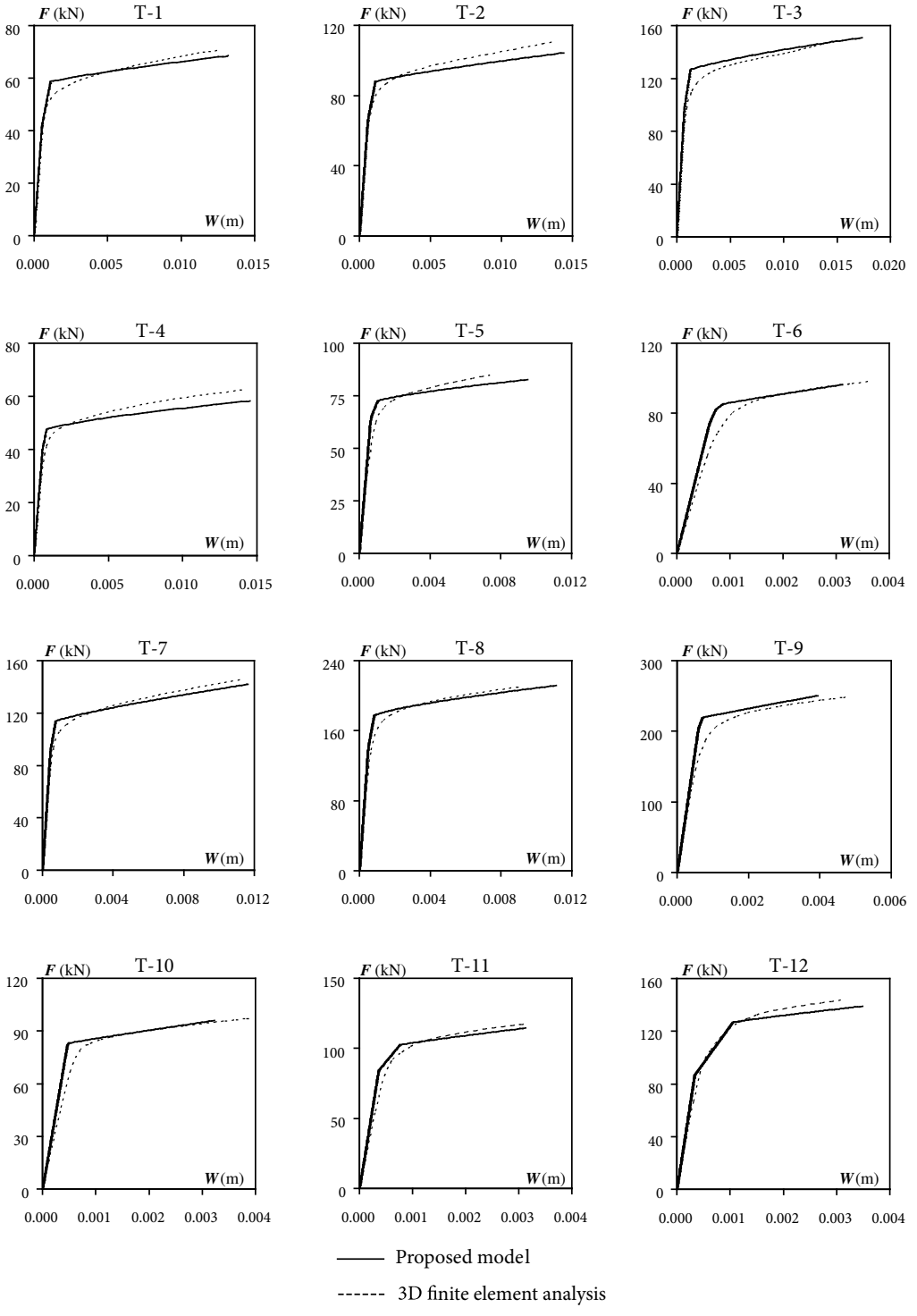

Figure 15. Force-displacement curves for the parametric study.

offers several advantages in this context by avoiding multiple cases and branches. The effectiveness of the model has been shown to be very satisfactory in evaluations comparing it to both experimental and numerical results. The solution time for a large number of load increments (500 or more) is negligible. Overall, the proposed model constitutes a valuable tool for the estimation of T-stub behavior, producing results comparable to much more complex and costly approaches such as 3D finite element analysis.

7. Notation

A	flange cross-sectional area
b	T-stub width
b_{eff}	effective T-stub width used for displacement calculations
c_b	axial stiffness of the bolt
d	distance between web face and bolt axis
d_b	bolt diameter
d_h	bolt head diameter
dF	incremental applied force
dF_b	incremental bolt force
dM_A	incremental bending moment at flange point A
dM_B	incremental bending moment at flange point B
$dM_{C^{i+1}}$	incremental bending moment at flange point C^{i+1}
dR	incremental prying force
dw	incremental transverse T-stub displacement
$dw_{j0\cdots2}$	parameters for the calculation of incremental displacement
dw_s	incremental transverse T-stub displacement due to shear
E	Young modulus
E^*	equivalent Young modulus
E_T	strain hardening modulus
E_T^*	equivalent strain hardening modulus
F	applied force
F_b	bolt force
f_u	ultimate stress
f_u^*	equivalent ultimate stress
f_y	yield stress
f_y^*	equivalent yield stress

G	shear modulus
G_1, G_2	parameters for the calculation of T-stub incremental response
I	moment of inertia
i	superscript indicating the loading step number
j	index indicating the trapezoid in numerical calculation of Int
Int	integral derived from flexural stiffness equivalence in flange-to-web fitting
k	number of trapezoids in numerical calculation of Int
L_0	flange length from edge A to start of plastification length
L_1	flange length from edge A to bolt axis
L_2	flange separation length measured from bolt axis to edge C
L_b	bolt shank length
L_c	equivalent flange-to-web fitting length
L_{pA}	plastification length near edge A
$L_{pB,1}$	plastification length at point B and towards the web
$L_{pB,2}$	plastification length at point B and towards the flange edge
M	flange bending moment
$M(x)$	flange bending moment function of x
M_2	flange plastification moment in bilinear representation
$M_2(x)$	flange plastification moment function of x
M_A	bending moment at flange point A
M_B	bending moment at flange point B
$M_{C^i}, M_{C^{i+1}}$	bending moment at flange point C^i and C^{i+1}
M_u	flange ultimate moment
M_y	flange yield moment
m	distance between bolt axis and an offset of web face by $0.8r$
$m_{j0\cdots5}$	parameters for the calculation of separation length
n	distance between bolt axis and flange edge
$p_{j0\cdots3}$	parameters for the calculation of T-stub incremental response
$q_{j0\cdots4}$	parameters for the calculation of T-stub incremental response
R	prying force
r	fillet radius of the flange-to-web fitting
$s_{j0\cdots2}$	parameters for the calculation of T-stub incremental response

t_f	flange thickness
$t_f(x)$	flange thickness function of x in flange-to-web fitting
$t_{f,j}$	flange thickness in trapezoid j
w	transverse T-stub displacement
w_b	bolt shank elongation
ε	strain
ε_b	strain at tensile fiber of bolt shank due to bending
$\varepsilon^p_{\text{eff}}$	effective plastic strain
ε_t	strain at tensile fiber of bolt shank due to tension
ε_u	ultimate strain
ε_y	yield strain
$\varepsilon_{xx}, \varepsilon_{yy}, \varepsilon_{zz}$	normal strains along axes x, y and z
$\varepsilon^p_{xx}, \varepsilon^p_{yy}, \varepsilon^p_{zz}$	normal plastic strains along axes x, y and z
ΔM_B	variation of flange bending moment at bending moment due to distributed bolt action
λ	parameter for the calculation of T-stub incremental response
υ	Poisson's ratio
σ	stress
σ_{eff}	effective stress
$\sigma_{xx}, \sigma_{yy}, \sigma_{zz}$	normal stresses along axes x, y and z
ϕ_B	flange rotation at bolt axis
ϕ_C	flange rotation at flange edge

References

[ADINA 2004] "ADINA theory and modeling guide, I: ADINA solids and structures", ADINA R&D Inc., Watertown, MA, 2004.

[Agerskov 1976] H. Agerskov, "High strength bolted connections subjected to prying", *J. Struct. Div.* (*ASCE*) **102**:1 (1976), 161–175.

[Beg et al. 2004] D. Beg, E. Zupancic, and I. Vayas, "On the rotation capacity of moment connections", *J. Constr. Steel Res.* **60**:3–5 (2004), 601–620.

[Bursi and Jaspart 1997] O. S. Bursi and J. P. Jaspart, "Calibration of a finite element model for isolated bolted end-plate steel connections", *J. Constr. Steel Res.* **44**:3 (1997), 225–262.

[CEN 2003] *Eurocode 3: Design of steel structures, 1.8: Design of joints*, Comité Européen de Normalisation (CEN), Brussels, Belgium, 2003. Stage 49 Draft.

[Chen and Han 1988] W. F. Chen and D. J. Han, *Plasticity for structural engineers*, Springer, New York, 1988.

[Girão Coelho et al. 2004] A. M. Girão Coelho, L. Simões da Silva, and F. Bijlaard, "Characterization of the nonlinear behaviour of single bolted T-stub connections", pp. 53–120 in *Proceedings of the Fifth International Workshop on Connections: Connections in steel structures, behavior, strength and design*, AISC-ECCS, Amsterdam, 2004.

[Faella et al. 2000] C. Faella, V. Piluso, and G. Rizanno, *Structural steel semirigid connections: Theory, design and software*, CRC Press, Boca Raton, FL, 2000.

[Gantes and Lemonis 2003] C. J. Gantes and M. E. Lemonis, "Influence of bolt length in finite element modeling of T-stub steel connections", *Comput. Struct.* **81**:8–11 (2003), 595–604.

[Huber and Tschemmernegg 1998] G. Huber and F. Tschemmernegg, "Modelling of beam-to-column joints", *J. Constr. Steel Res.* **45**:2 (1998), 199–216.

[Jaspart 1991] J. P. Jaspart, *Étude de la semi-rigidité des noeuds pouter-colonne et son influence sur la résistance et la stabilité des ossatures en acier*, Ph.D. thesis, University of Liège, Belgium, 1991.

[Kuhlmann and Kuhnemund 2000] U. Kuhlmann and F. Kuhnemund, "Procedures to verify rotation capacity", pp. 167–226 in *Semi-rigid connections in structural steelwork*, edited by M. Ivanyi and C. C. Banitopoulos, CISM Courses and Lectures **419**, Springer, Vienna, 2000.

[Mistakidis et al. 1997] E. S. Mistakidis, C. C. Baniotopoulos, C. D. Bisbos, and P. D. Panagiotopoulos, "Steel T-stub connections under static loading: An effective 2-D numerical model", *J. Constr. Steel Res.* **44**:1–2 (1997), 51–67.

[Sherbourne and Bahaari 1996] A. N. Sherbourne and M. R. Bahaari, "3D simulation of bolted connections to unstiffened columns, I: T-stub connections", *J. Constr. Steel Res.* **40**:3 (1996), 169–187.

[Shi et al. 1996] Y. J. Shi, S. L. Chan, and Y. L. Wong, "Modeling for moment-rotation characteristics for end-plate connections", *J. Struct. Eng.* (*ASCE*) **122**:11 (1996), 1300–1306.

[Swanson and Leon 2001] J. A. Swanson and R. T. Leon, "Stiffness modeling of bolted T-stub connection components", *J. Struct. Eng.* (*ASCE*) **127**:5 (2001), 498–505.

[Wanzek and Gebbeken 1999] T. Wanzek and N. Gebbeken, "Numerical aspects for the simulation of end plate connections", pp. 13–31 in *Cost C1 WG6 report: Numerical simulation of semi-rigid connections by the finite element method*, edited by K. S. Virdi, European Commission, Brussels, 1999.

[Weynand et al. 1995] K. Weynand, J. Jaspart, and M. Steenhuis, "The stiffness model of revised annex J of Eurocode 3", pp. 441–452 in *Connections in steel structures III: Proceedings of the Third International Workshop on Connections in Steel Structures* (Trento, Italy), edited by R. Bjorhovde et al., Pergamon, Tarrytown, NY, 1995.

[Yee and Melchers 1986] Y. L. Yee and R. E. Melchers, "Moment-rotation curves for bolted connections", *J. Struct. Eng.* (*ASCE*) **112**:3 (1986), 615–635.

[Zoetemeijer 1974] P. Zoetemeijer, "A design method for the tension side of statically loaded, bolted beam-to-column connections", *Heron* **20**:1 (1974), 1–59.

Received 29 Dec 2005. Revised 5 May 2006. Accepted 19 Jun 2006.

MINAS E. LEMONIS: mlemonis@central.ntua.gr
National Technical University of Athens, Laboratory of Steel Structures, 9 Iroon Polytechniou, 157 80, Zografou, Greece

CHARIS J. GANTES: chgantes@central.ntua.gr
National Technical University of Athens, Laboratory of Steel Structures, 9 Iroon Polytechniou, 157 80, Zografou, Greece